International Journal of Environmental Sciences
ISSN: 2229-7359
Vol. 11 No. 23s, 2025
https://www.theaspd.com/ijes.php

Synthesis, Characterization And Thermal Decomposition Of N-(3-Butyl-2, 6-Diphenylpiperidin-4-Ylidene)Isonicotinohydrazide-Non-Isothermal Condition

Govindasamy Vallal Perumal[a], V Jayavel Ramya Devi[a], Govindasamy Rajarajan[a,b*] and Venugopal Thanikachalam[a]

[a]*Department of Chemistry, Annamalai University, Annamalainagar-608002, India;*
[b*]*Department of Chemistry, Bharathiar University, Coimbatore-641046, India*

Graphical abstract

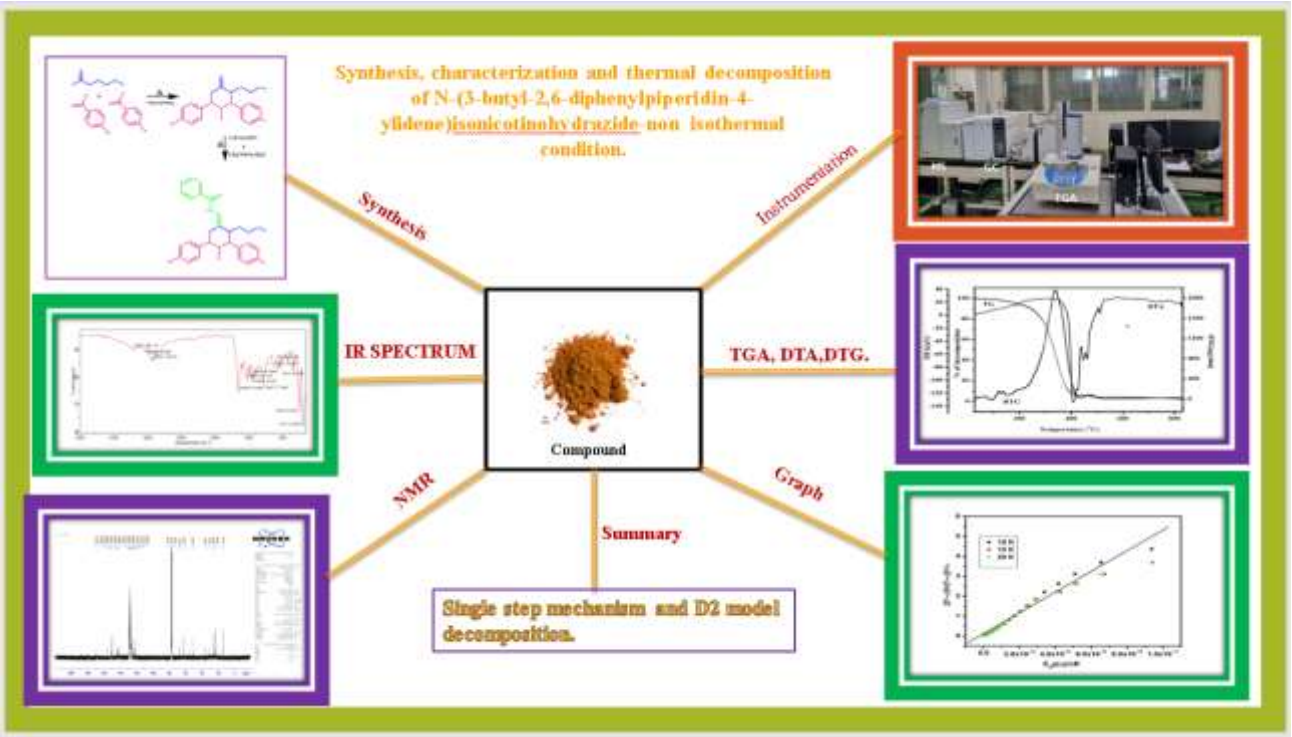

Abstract

Background: *The compound N-(3-butyl-2,6-diphenylpiperidin-4-ylidene)isonicotinohydrazide (BDPINH) was synthesized through a condensation reaction involving piperidin-4-one, isoniazid and sodium acetate trihydrate in an ethanol medium. The reaction mixture was refluxed at 80°C for 12 hours.*

Objective: *The resulting product was characterized using FT-IR and NMR spectroscopies. To investigate its thermal behavior, thermal decomposition studies were performed using a system combined with thermogravimetric analysis (TG), differential thermal analysis (DTA) and differential thermogravimetric analysis (DTG) under a dynamic nitrogen atmosphere across variable temperatures.*

Methods: *Kinetic and thermodynamic parameters were derived using iso-conversional model-free methods such as the Friedman, Kissinger-Akahira-Sunose (KAS) and Flynn-Wall-Ozawa (FWO) . Additionally, the Coats–Redfern method was used for model-fitting analysis.*

Results: *The TG curves indicated a single-step decomposition pathway. Activation energy (Ea) values and correlation coefficients (r) were calculated and graphically represented using the isoconversional techniques. Theoretical reaction models were compared with the experimental data, revealing that the compound decomposes follow a two-dimensional diffusion mechanism (D2 model).*

Conclusion: *Both kinetic and thermodynamic parameters were compiled in table form and visualized through the graphical plots.*

International Journal of Environmental Sciences
ISSN: 2229-7359
Vol. 11 No. 23s, 2025
https://www.theaspd.com/ijes.php

Keywords: *Isoniazid, TG, DTA, DTG, Friedmann, KAS, FWO, model fitting analysis and D2 model.*

1. INTRODUCTION

Hydrazones serve as crucial intermediates in the synthesis of diverse heterocyclic compounds and are known for their broad spectrum of biological activities. These compounds have a wide range of applications, including use as plant preservatives, pharmaceutical agents, polymer production components, adhesives and in various industrial processes [1]. Numerous biologically active hydrazide-hydrazone derivatives containing various functional groups have been synthesized from a wide range of carbonyl compounds. These derivatives have deep-rooted potential as anticancer agents [2]. Hydrazones were characterized by the functional group (-C(=O)-NH-NH_2) and essential intermediates. Acid hydrazides and their derivatives serve as important building blocks structure for five, six or seven-membered heterocyclic rings that include one or more heteroatoms [3]. Hydrazones possess a structure that includes nucleophilic imine and highly reactive amino-type nitrogen atoms, along with an imine carbon exhibiting both electrophilic and nucleophilic behavior. The presence of the C=N double bond leads to configurational isomerism and in most cases, an acidic N-H proton is also present. These structural features significantly influence the chemical and physical characteristics of hydrazones that are typically synthesized through the condensation reaction of a hydrazine or hydrazide with an aldehyde or ketone. Isoniazid, a derivative of isonicotinic acid and well-established as a potent agent against tuberculosis and continues to be utilized for both treatment and prevention. However, current isoniazid-based formulations are often associated with a range of adverse side effects. Interestingly, studies have shown that hydrazones formed by reacting isoniazid with certain hydroxy-aldehydes retain their therapeutic effectiveness while exhibiting reduced toxicity [4,5]. Isonicotinic acid, also referred to as pyridine-4-carboxylic acid, is an isomer of both picolinic acid and nicotinic acid (vitamin B_2 or niacin). It contains two potential donor atoms the nitrogen in the pyridine ring and the oxygen in the carboxyl group which can coordinate with metal centers in various modes, including functioning as monodentate ligands or forming bridging interactions between metal atoms[6]. Isoniazid (isonicotinic hydrazide, INH) is a key antitubercular agent commonly used in combination with ethambutol, rifampin, streptomycin and pyrazinamide for the treatment of tuberculosis. Although numerous isoniazid-based compounds have been synthesized and evaluated, the ongoing emergence of antibiotic-resistant bacterial strains continues to drive the demand for new derivatives with improved efficacy[7,8]. Aryl hydrazone-based coordination compounds have been identified as potential enzyme inhibitors. Isoniazid a well-established therapeutic agent is widely used to treat various bacterial infections, particularly tuberculosis[9-12]. Hydrazones formed through the condensation of isoniazid with pyridine-based aldehydes have demonstrated enhanced antitubercular activity compared to INH[13]. However, current formulations are associated with various adverse side effects and in some chronic cases, may lead to irreversible liver damage. These limitations, along with the growing resistance of microorganisms to existing treatments, have prompted the development of new therapeutically effective compounds[14,15]. Although considerable research has been conducted, the exploration of how small molecules interact with DNA continues, aiming to discover highly selective and effective therapeutic agents. Numerous intercalating compounds and groove-binding molecules have been identified for their potential in treating viral infections, tumors, bacterial and fungal diseases[16]. The pharmacological behavior of metal complexes is largely influenced by the type of metal ions and the nature of the coordinating ligands. Numerous studies have reported that ligands when combined with different metal ions form complexes that display a wide range of biological activities [17,18]. Building upon the structural and therapeutic features of isoniazid (INH), quinoline and pyridine the design of INH carbohydrazide derivatives offers a capable strategy for achieving multiple therapeutic effects. These compounds have the potential to retain the antimicrobial efficacy of INH while incorporating additional functionalities that contribute to anti-inflammatory and anti-diabetic activities. This makes them auspicious candidates for the treatment of conditions involving both metabolic and exciting components. The synthesis of such derivatives typically involves purposeful chemical modifications designed at improving solubility, stability and bioavailability, thereby overcoming some of the drawbacks associated with conventional therapies and enhancing overall treatment effectiveness[19-26]. In the search for new antileishmanial agents, focused on the design and synthesis of novel pyrimidinylhydrazone and pyrimidinyl-N-acylhydrazone derivatives. These compounds were synthesized to evaluate their antileishmanial activity *in vitro* and to investigate their possible mechanisms of action. Recently, interest has grown in developing hydrazone and acylhydrazone derivatives with diverse core structures for combating leishmaniasis. López and co-workers reported the creation of 4-chloro-1-phthalazinyl hydrazone derivatives that demonstrated activity against

Leishmania braziliensis [27]**.** During isoniazid synthesis, Schiff base complexes are often formed through condensation reactions with compounds that contain aldehyde or ketone groups. These methods was investigatived the reactive sites, offering insights into the mechanisms underlying their antioxidant and antibacterial properties, as well as the energetic aspects of the associated chemical reactions **[28].** Thermal vaporization behavior of (*E*)-methyl-2-hydroxy-5-(phenyldiazenyl)benzoate under non-isothermal conditions in an air atmosphere reported by Nagendra Babu et al. [29]**.**The paper aims to confirm the thermal stability of N-(3-butyl-2,6-diphenylpiperidin-4-ylidene)isonicotinohydrazide (BDPINH) by thermally vaporizing it in a nitrogen atmosphere under non-isothermal condition.

2. EXPERIMENTAL

2.1 Materials and reagents

Analytical-grade reagents of high purity such as benzaldehyde, 2-heptanone, ammonium acetate, sodium acetate trihydrate and isoniazid were utilized for the synthesis. Melting points were measured using open capillary tubes. The progress of reactions was monitored by thin layer chromatography (TLC) on Merck pre-coated silica gel 60 F254 aluminum plates, employing a petroleum ether and ethyl acetate solvent system for spot development. Infrared (IR) spectrum was collected using a Thermo Nicolet AVATAR-330 FT-IR spectrometer. Proton (^{1}H) and carbon (^{13}C) nuclear magnetic resonance (NMR) spectra were recorded on a Bruker instruments operating at 400 MHz and 100 MHz, respectively. Tetramethylsilane (TMS) served as the internal standard and chemical shifts were expressed in δ (ppm). Signal multiplicities in ^{1}H NMR included singlet (s), doublet (d), doublet of doublets (dd), triplet (t), quartet (q) and multiplet (m). Thermal behavior was investigated using a simultaneous thermogravimetric and differential thermal analysis system (STA 7200, Hitachi HTG, Japan) at Vignan University, Vadlamudi, Andhra Pradesh (Tenali Road, Guntur, 522213). Analyses (TG, DTA, and DTG) were performed in ceramic crucibles under static nitrogen gas (flow rate: 100 mL/min), with approximately 8 mg of sample heated from 23 to 700°C at rates of 10, 15 and 20°C. The sample temperature, regulated by a thermocouple, consistently followed the programmed heating profile. Dedicated software was employed to determine kinetic parameters such as activation energy (E_a) and the logarithmic pre-exponential factor (ln A).

2.2 Synthesis of N-(3-butyl-2,6-diphenylpiperidin-4-ylidene)isonicotinohydrazide:

A mixture of ammonium acetate (0.05 mol), benzaldehyde (0.1 mol), and 2-heptanone (0.05 mol) in ethanol was refluxed. The reaction mixture, on cooling, afforded a viscous residue which was dissolved in ether (200 mL) and treated with concentrated HCl (10 mL). The resulting hydrochloride salt of 3t-butyl-2r,6c-diarylpiperidin-4-one was collected by filtration, washed with ethanol–ether (1:1) followed by ether, and converted to the free base using aqueous ammonia. The crude product was diluted with water and recrystallized from ethanol to give the pure compounds [30]. A condensation reaction was carried out using 0.01 mol of 3-butyl-2,6-diphenylpiperidin-4-one and 0.02 mol of isoniazid in the presence of 0.01 mol of sodium acetate trihydrate**[31]**, maintaining a molar ratio of 1:2:1. The reaction was conducted in ethanol as the solvent and refluxed at 80°C for 10-12 hours. The progress of the reaction was tracked using the thin layer chromatography (TLC). Upon completion, the reaction mixture was poured into a dry ice bath, resulting in the formation of a precipitate. The crude product was then purified by recrystallization from ethanol to obtain the final compound in its pure form. The yield of the reaction ranged between 70-80%. The synthetic pathway is illustrated in **Scheme 1**.

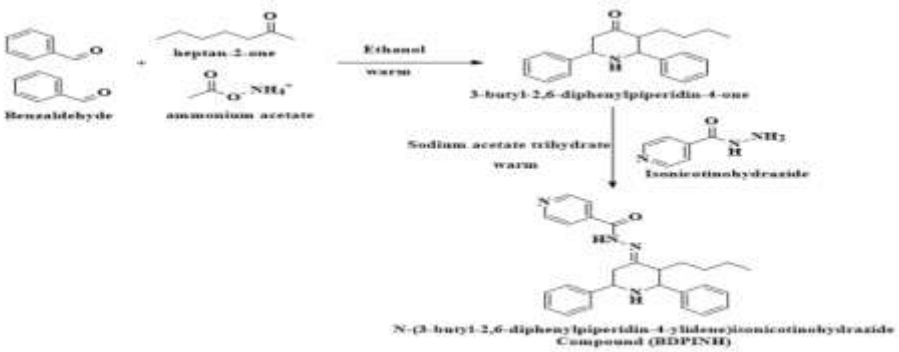

Scheme 1. Scheme of the synthetic route of BDPINH

International Journal of Environmental Sciences
ISSN: 2229-7359
Vol. 11 No. 23s, 2025
https://www.theaspd.com/ijes.php

2.3 FT-IR spectral analysis of BDPINH

The synthesised compound N-(3-butyl-2,6-diphenylpiperidin-4-ylidene)isonicotinohydrazide (BDPINH) exhibits distinct FT-IR spectral features that elucidate its structural framework. The N-H stretching vibrations observed in the range of 3220 cm^{-1} confirm the presence of amine groups, indicative of nitrogen–hydrogen bonding. Aliphatic C-H stretching bands, appearing in 2929 cm^{-1} suggested the incorporation of aliphatic chains, specifically the butyl moiety into the molecular structure. A prominent C=O stretching band at 1654 cm^{-1} confirms the presence of a amide carbonyl group. The C=N stretching vibrations detected in the 1520 cm^{-1} region indicate the existence of carbon–nitrogen double bonds, which play a significant role in defining both the reactivity and structural integrity of the compound. Additionally, C-N stretching absorptions observed between 1289 cm^{-1}, along with the out-of-plane bending vibrations of aromatic C–H bonds in the 700-842 cm^{-1} range support the presence of substituted diphenylpiperidine moieties. These spectral features collectively confirmed the functional groups such as aromatic rings, C=N, NH groups and aliphatic side chains. FT-IR analysis provides wide-ranging insight into the molecular structure and functional group of the synthesized compound Fig. (1).

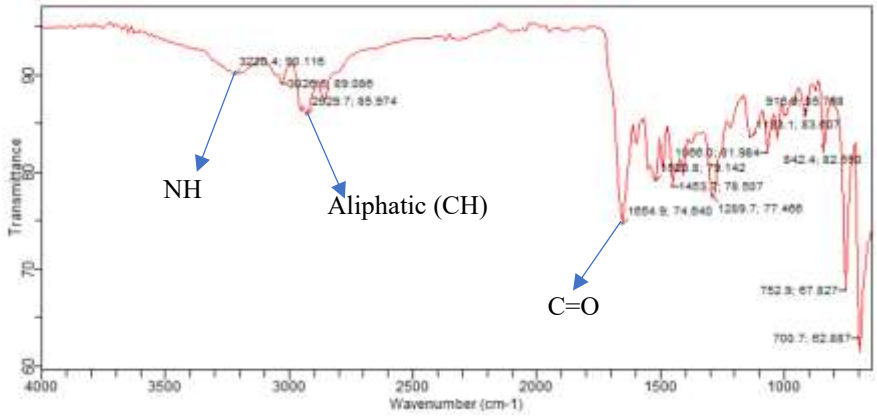

Fig. (1). FT-IR Spectrum of BDPINH

2.4 ^{1}H NMR Spectral analysis of BDPINH

In the ^{1}H NMR spectrum, the methylene protons of the butyl group appeared as multiplets within the 0.89-1.25 ppm range, integral for eight protons. Aromatic proton resonances were detected between 7.26-7.65 ppm and NH proton appeared at 8.74ppm. Signals at 4.04 and 3.61 ppm were assigned to the benzylic protons at H(6) and H(2), respectively. The axial methylene proton H(5a) resonated at 1.60 ppm, while the equatorial methylene proton H(5e) appeared at 2.61 ppm. The H(3) proton was observed between 2.19 and 2.37 ppm. An upfield triplet at 0.73 ppm corresponded to the methyl protons of the butyl side chain. This conformation is illustrated in Fig. (2), offering strong spectroscopic evidence for the proposed structure and stereochemistry of the synthesized compound.

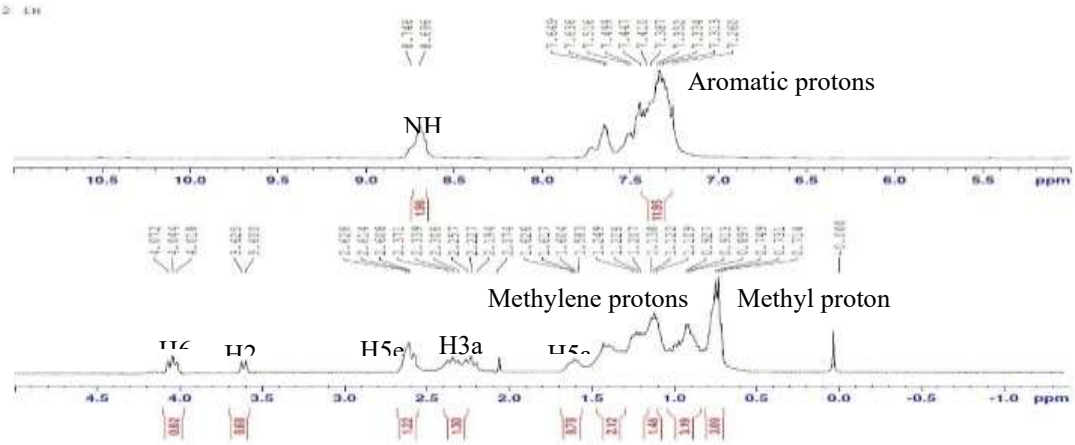

Fig. (2). ^{1}H NMR Spectrum of BDPINH.

2.5 ^{13}C NMR spectral analysis of BDPINH

In ^{13}C NMR spectrum of the compound shows aromatic carbon signals in the range of 121.19-142.95 ppm. Methyl carbon appear in a narrow region around 13.86 ppm, while methylene carbons resonate between 22.89 and 29.91 ppm, reflecting their distinct structural environments. A signal at 67.22 ppm corresponds to the C(2) carbon, whereas C(5) is observed near 36.16 ppm. The C=O carbon gives a notably downfield peak at 169.43 ppm, suggesting strong deshielding effects possibly due to conjugation or electron-withdrawing groups. Resonances for C(3) and C(6) are detected at 51.59 ppm and 61.87 ppm, respectively. Ipso carbons, generally appearing at higher frequencies than other aromatic carbons, are found between 149.47 and 150.56 ppm. A distinct downfield peak at 156.14 ppm is assigned to the C4 carbon of the isonicotinic hydrazide group in the Fig. (3).

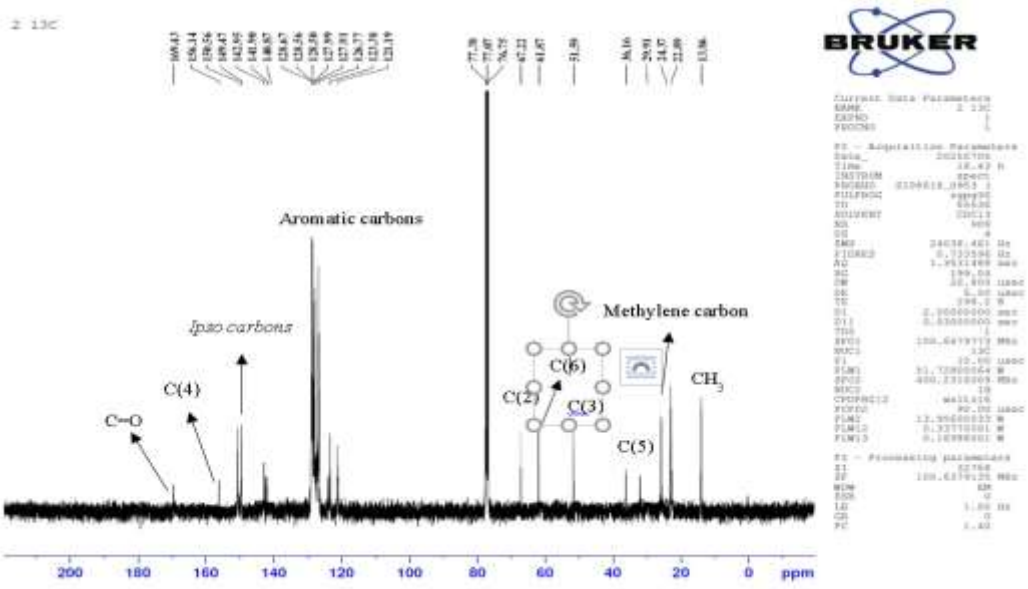

Fig. (3). ^{13}C NMR Spectrum of BDPINH.

2.6. Model-free isoconversional methods

In thermogravimetric analysis, the conversion (α) is defined as the ratio of the measured mass loss at a given stage to the total mass loss corresponding to the entire process under investigation.

$$\alpha = \frac{m_0 - m_t}{m_0 - m_f}$$

Here m_t, m_0 and m_f represent the definite mass at a given temperature, the initial mass and the final mass of the compound, respectively.

2.6.1 Friedman's method

Friedman's[32] isoconversional (model-free) method is used to analyze the effect of activation energy (E_a) on the degree of conversion (α). The activation energy and frequency factor are obtained from the slope and intercept, respectively of the linear plot of the $\ln\left(\beta\frac{d\alpha}{dT}\right)$ *versus* the inverse of temperature (1/T).

$$\ln\left[\beta\frac{d\alpha}{dT}\right] = \ln[A_\alpha f(\alpha)] - \frac{E_{a,\alpha}}{RT_\alpha} \quad \ldots (1)$$

2.6.2 Flynn-Wall-Ozawa (FWO) method

The FWO[33] method is a model-free technique that involves plotting ln β *versus* 1/T data to calculate the activation energy (E_a) from the slope of the plots, using temperatures at fixed conversion levels obtained from experiments carried out at different heating rates β.

$$\ln \beta = \ln\left[\frac{0.0048\,AE_a}{g(\alpha)\,R}\right] - 1.0516\frac{E_a}{RT} \qquad \ldots (2)$$

2.6.3 Kissinger-Akahira-Sunose (KAS) method

The Kissinger-Akahira-Sunose (KAS)[34] method is a kinetic analysis technique that establishes the relationship between activation energy and degree of conversion for dynamic studies at various constant heating rates. The Plotting of ln (β/T^2) versus 1/T can appropriate conversion role results in a linear relationship, the slope and intercept of which are used to determine the activation energy and frequency factor.

$$\ln\left(\beta / T^2\right) = \ln\left[\frac{AE_a}{g(\alpha)\,R}\right] - \frac{E_a}{RT} \qquad \ldots (3)$$

2.7 Model-fitting method

Model-fitting kinetic parameters were calculated using almost fifteen models in the Coats-Redfern[35] algorithm. Among these, the model with the highest linearity was selected. The resulting linear plot ln [($g(\alpha)$)/T^2] *versus* 1/T provided the pre-exponential factor and activation energy derived from the intercept and slope respectively.

$$\ln\left[\frac{g(\alpha)}{T^2}\right] = \ln\left(\frac{AR}{\beta E_a}\left[1-\left(\frac{2RT^*}{E_a}\right)\right]\right) - \frac{E_a}{RT} \qquad \ldots (4)$$

The Kissinger method uses the temperature at which the reaction rate is maximum(peak temperature-T_m) [36], obtained from experiments at different heating rates.

$$\ln\left(\frac{\beta}{T_m^2}\right) = -\frac{E_a}{RT_m} + \ln\left(\frac{AR}{E_a}\right) \qquad \ldots (5)$$

The frequency factor and thermodynamic parameters such as enthalpy of activation $\Delta H^{\neq}$, entropy of activation $\Delta S^{\neq}$ and Gibbs free energy of activation $\Delta G^{\neq}$ are estimated using the following equations:[37-42]

$$A = \frac{e\chi k_B T_p}{h}\exp\left(\frac{\Delta S^{\neq}}{R}\right) \qquad \ldots (6)$$

$$\Delta S^{\neq} = R \ln \frac{Ah}{e\chi k_B T_p} \qquad \ldots (7)$$

$$\text{Since } \Delta H^{\neq} = E_a - RT_p \qquad \ldots (8)$$

$$\Delta G^{\neq} = \Delta H^{\neq} - T_p \Delta S^{\neq} \qquad \ldots (9)$$

Where R (R= 8.314 $JK^{-1}mol^{-1}$) is the gas constant, h (h = 6.626 x 10^{-34} J sec^{-1}) is the Planck constant, k_B(k_B= 1.38 x $10^{-23}JK^{-1}$) is the Boltzman constant, Tp is the peak temperature of the DTG curve.

3. RESULTS AND DISCUSSION

The compound undergoes decomposition in a single step, as indicated by the thermogravimetric (TG) curves recorded at heating rates of 10, 15, and 20°C min^{-1} (Fig. 4a-c). The TG data reveal that the compound starts melting at 74°C and begins to decompose near 200°C. The peak observed in the curves corresponds to the weight loss occurring during the heating process from room temperature up to 200°C, continuing until 455°C.Additionally, increasing the heating rate causes the peak decomposition temperature to shift toward higher temperatures in all the asymmetric TG curves. The thermal behavior of the compound was primarily investigated through non-isothermal decomposition using model-free approaches including the Friedmann's[32], Flynn-Wall-

Ozawa (FWO)[33] and Kissinger-Akahira-Sunose methods[34]. The data reveal the variation of the apparent activation energy (Ea) for compound as a function of the degree of conversion (α). Within the conversion range of 0.20 to 0.90, the E_a initially decreases slightly and then rises with increasing conversion (Table 1). The E_a values obtained from both the Friedman and Flynn-Wall-Ozawa (FWO) isoconversional methods are in closer confirmation. Additionally, the results indicate that the apparent activation energy depends on the extent of conversion(α) contributing to a deeper insight into the complicated decomposition process and determination of its mechanism. The Friedman method estimates the average activation energy (E_a) for decomposition as 91.88 ± 2.11 kJ mol^{-1} over the conversion range of 0.10 to 0.90. The activation energies derived from the Friedman method are relatively close to those obtained by the Flynn-Wall-Ozawa (FWO) method and show better consistency with the Kissinger-Akahira-Sunose (KAS) method. Within this conversion interval, the activation energy varies slightly regardless of the calculation technique used, with average E_a values of 91.88 ± 2.11, 94.31± 0.21 and 96.06 ± 0.21 kJ mol^{-1} for the Friedman, KAS and FWO methods respectively.

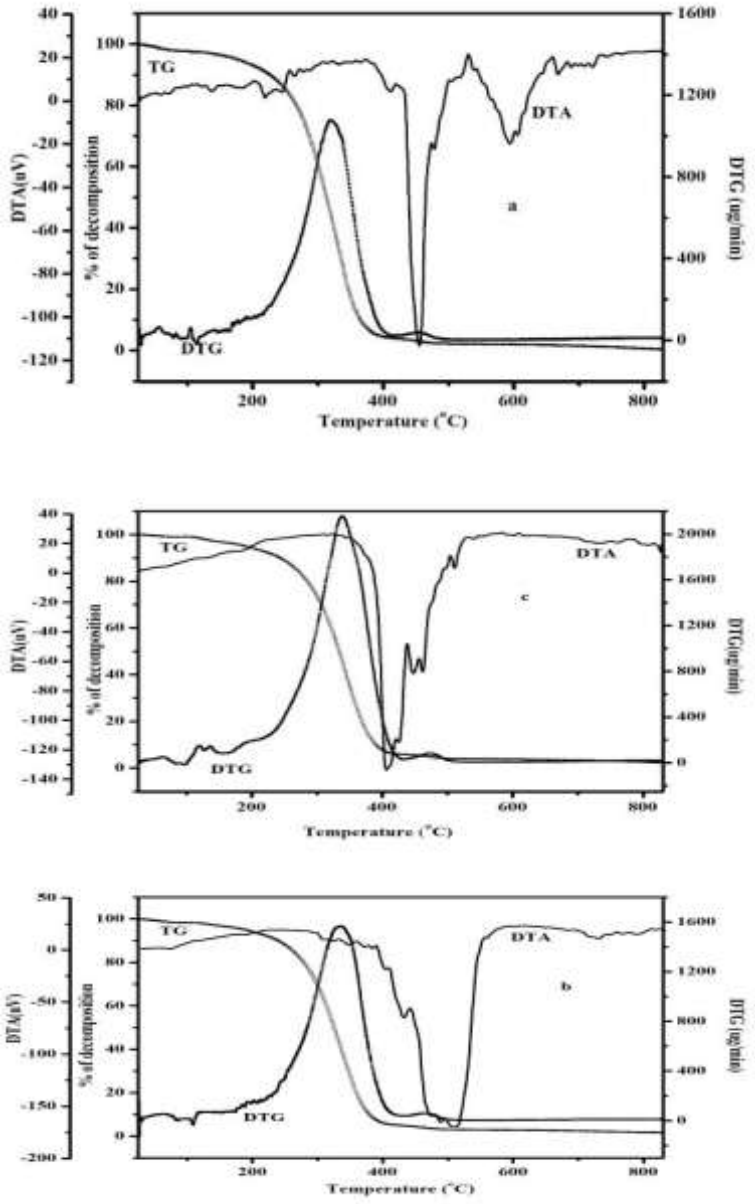

Fig .(4). TG, DTG and DTA curves of BDPINH in nitrogen atmasphere at a) 10°C/min; b) 15°C/min c) 20°C/min

International Journal of Environmental Sciences
ISSN: 2229-7359
Vol. 11 No. 23s, 2025
https://www.theaspd.com/ijes.php

Table 1, Temperatures corresponding to the same degree of conversion at different heating rates for BDPINH.

α	Temperature (K)			Friedman method		KAS method		FWO method	
	10 (°C/min)	15 (°C/min)	20 (°C/min)	E_a (kJ mol^{-1})	r	E_a (kJ mol^{-1})	r	E_a (kJ mol^{-1})	r
0.05	449.9	461.5	462.2			73.65	-0.915	77.01	-0.930
0.1	499.6	513.1	516.2	72.47	-0.973	74.37	-0.957	77.70	-0.968
0.15	525	536.5	542	95.08	-0.999	87.76	-0.99	89.60	-0.994
0.2	541.1	552.8	558.6	93.38	-0.996	90.91	-0.991	92.71	-0.995
0.25	552.4	564.3	570.4	93.12	-0.997	92.41	-0.992	94.18	-0.996
0.3	561	573.3	579.5	90.83	-0.993	92.53	-0.992	94.43	-0.995
0.35	568.5	580.3	587.7	89.65	-0.984	93.38	-0.997	94.77	-0.999
0.4	575.1	587.4	594.6	92.43	-0.99	93.51	-0.996	95.16	-0.998
0.45	581.4	593.6	601.3	92.92	-0.999	94.23	-0.997	95.71	-0.999
0.5	586.5	598.8	606.7	93	-1	94.58	-0.998	96.04	-0.999
0.55	591.6	604.1	612.1	92.81	-0.999	94.78	-0.998	96.29	-0.999
0.6	596.6	610.2	617.3	89.58	-0.922	93.66	-0.992	95.84	-0.996
0.65	601.9	615.2	623.2	88.14	-0.985	93.85	-0.996	95.70	-0.999
0.7	607.0	620.8	628.6	90.62	-0.984	93.55	-0.995	95.65	-0.998
0.75	613.3	626.9	635.3	94.02	-0.997	94.51	-0.997	96.37	-0.999
0.8	619.5	633	641.8	96.3	-0.999	95.55	-0.998	97.27	-0.999
0.85	627.5	641.8	650.4	89.87	-0.988	94.75	-0.996	96.84	-0.999
0.9	639.2	653.1	663.1	91.51	-0.989	95.48	-0.999	97.10	-1.000
				91.88 ± 2.11		**94.31±0.21**		**96.06 ± 0.21**	

3.1 Model-fitting analysis

Each of the 15 models [35] are listed in Table 2 was fitted to the non-isothermal kinetic data of the compound within the conversion range of $0.10 \leq \alpha \leq 0.90$, where model-free analysis revealed an essentially constant activation energy. The chosen reaction model significantly impacts the calculated activation energy (E_a), pre-exponential factor (ln A), correlation coefficient (r), and the kinetic descriptions of the decomposition process. The invariant kinetic parameters method reinforces the findings from the kinetic data, confirming that the decomposition follows a single step mechanism.

Table 2, Determination of apparent activation parameters by Coats-Redfern method for each heating rate of BDPINH in the nitrogen atmosphere.

Kinetic model	β = 10 °C/min			β = 15 °C/min			β = 20 °C/min		
	E_a (kJ mol^{-1})	ln A (A/min)	r	E_a (kJ mol^{-1})	ln A (A/min)	r	E_a (kJ mol^{-1})	ln A (A/min)	r
P2	13.66	-0.61	-0.97	13.81	-0.27	-0.97	13.45	-0.14	-0.969
P3	5.84	-2.94	-0.928	5.87	-2.6	-0.927	5.58	-2.45	-0.92
P4	1.95	-4.78	-0.732	1.92	-4.45	-0.721	1.67	-4.37	-0.671
F1	61.84	10.81	-0.999	62.75	11.1	-0.999	61.88	11.02	-0.998
F2	97.2	19	-0.989	98.69	19.25	-0.989	97.45	19.01	-0.989
F3	141.54	29.04	-0.974	143.74	29.24	-0.975	142.04	28.8	-0.974
D1	94.62	24.44	-0.991	96.08	24.73	-0.991	95.07	24.57	-0.99
D2	97.29	16.94	-0.994	98.75	17.18	-0.994	97.52	16.95	-0.994
D3	114.64	19.43	-0.998	116.38	19.65	-0.998	114.96	19.34	-0.998
D4	103	16.75	-0.996	104.55	16.99	-0.996	103.25	16.73	-0.996
A2	26.03	2.77	-0.998	26.38	3.1	-0.998	25.89	3.18	-0.998
A3	14.08	-0.24	-0.997	14.24	0.1	-0.998	13.87	0.23	-0.997
A4	8.13	-1.98	-0.995	8.2	-1.63	-0.996	7.89	-1.49	-0.995
R2	48.17	6.85	-0.996	48.86	7.16	-0.996	48.14	7.14	-0.996
R3	44.36	6.2	-0.993	44.99	6.51	-0.993	44.3	6.51	-0.993

3.2 Invariant kinetic models

The invariant kinetic parameters method was applied to data collected at heating rates of 10, 15 and 20 K min^{-1}. The kinetic parameters were evaluated using the Coats-Redfern method, as summarized in Table 3. For these kinetic models, the Coats-Redfern [35] plots exhibit straight lines with correlation coefficients close to unity within the conversion range of $0.10 \leq \alpha \leq 0.90$. Table 3 illustrates that the values of E_a and ln A are influenced by both the heating rate and kinetic model. The pre-exponential factor and actual activation energy, collectively

known as invariant kinetic parameters, are determined by plotting ln A_{inv} versus E_{inv} across multiple constant heating rates. The resulting straight lines are expected to intersect at a unique point (E_{inv}, A_{inv})[43-45]. The evaluation of these parameters is carried out using the supercorrelation equation. Specifically, the plot of a_β versus b_β for three constant heating rates yields a straight line, from which ln A_{inv} and E_{inv} can be derived. The Erofe'v model stood out among all other models, with its apparent parameters determined by high correlation coefficients (Table 4).

Table 3, Compensation effect parameters for several combinations of kinetic models for BDPINH in the nitrogen atmosphere.

β (°C /min)	AKM			AKM–{P4,D1,D3,D4}		
	a_β (A/min)	b_β (mol J^{-1})	r	a_β (A/min)	b_β (mol J^{-1})	r
10	0.22923	-3.88605	0.979	0.22864	-3.79751	0.998
15	0.22464	-3.51966	0.979	0.22397	-3.42632	0.998
20	0.22289	-3.30290	0.978	0.22195	-3.18988	0.998
β (°C /min)	AKM-{P3,P4,D1,D3,D4}			AKM-{P2-P4, D1,D3,D4,A3,A4}		
	a_β (A/min)	b_β (mol J^{-1})	r	a_β (A/min)	b_β (mol J^{-1})	r
10	0.22678	-3.62758	0.997	0.22678	-3.62758	0.997
15	0.22211	-3.25338	0.998	0.22211	-3.25338	0.998
20	0.21999	-3.01050	0.997	0.21999	-3.01050	0.997

Table 4, Isokinetic parameters of kinetic models for BDPINH in the nitrogen atmosphere.

Kinetic model	E_{inv} (kJ mol^{-1})	ln A_{inv} (A/min)	-r
AKM	16.62 ± 2.14	89.51 ± 9.5	-0.995
AKM–{P4,D1,D3,D4}	16.50 ± 1.9	88.84 ± 8.6	-0.994
AKM-{P3,P4,D1,D3,D4}	16.57 ± 1.8	89.11 ± 8.1	-0.995
AKM-{P2-P4, D1,D3,D4,A3,A4}	16.55 ± 1.8	89.07 ± 8.3	-0.995

3.3 Determination of the kinetic model by master plots

The integral conversion function for solid-state non-isothermal decomposition reactions [46] is given by:

$$g(\alpha) = \frac{A}{\beta}\int_{T_0}^{T}\exp\left(-\frac{E_a}{RT}\right)dT = \frac{AE_a}{R\beta}p(u) \qquad ...(10)$$

where $p(u) = \int_{\infty}^{u}\frac{exp(-u)}{u^2}du$ and $u=E_a/RT$

Using α=0.5 as the reference point, and according to the FWO method, the following expression is obtained:

$$g(\alpha_{0.5}) = \left(\frac{AE_a}{\beta R}\right)p(u_{0.5}) \qquad ...(11)$$

Plots of $g(\alpha)/g(\alpha_{0.5})$ against α correspond well with the master plots of various hypothetical $g(\alpha)$ functions listed in Table 4. An accurately estimated formula [46] is used to construct experimental master plots of $p(u)/p(u_{0.5})$ using data obtained at different heating rates:

$$\frac{g(\alpha)}{g(\alpha_{0.5})} = \frac{p(u)}{p(u_{0.5})} \qquad .....(12)$$

$$p(u) = \exp(-u)/\ [u(1.00198882u+1.87391198)] \qquad .....(13)$$

According to Eq. (13), when the correct kinetic model is applied, the experimental values of $g(\alpha)/g(\alpha_{0.5})$ are consistent for a given α. Therefore, the kinetic model can be identified by comparing the theoretical and experimental master plots Fig. (5). The kinetic model associated with the thermal decomposition of the

compound was determined by comparing the experimental master plots with their theoretical counterparts **[47,48].** To verify the decomposition mechanism, master plots of various kinetic functions versus α were generated from experimental data obtained for the decomposition stages at different heating rates in an air atmosphere. The comparison revealed that the decomposition stage of the compound corresponds to the D2**[49]** master curve. By assuming the theoretical D2 model, the logarithm of the pre-exponential factor (ln A) for the decomposition stage was determined from the correlation coefficient of the plots of $[(1-\alpha)\ln(1-\alpha)]+\alpha$ *versus* $E_a p(u)/\beta R$ resulting in a value of 16.55 ±1.8.

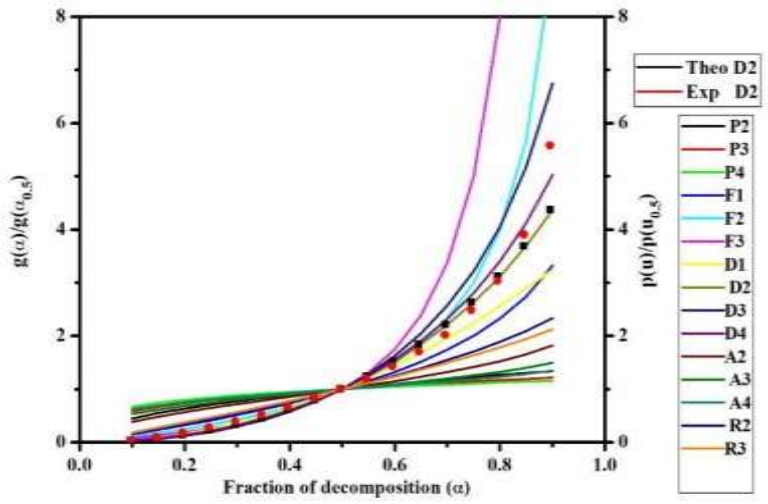

Fig .(5). Plot of $g(\alpha)/g(\alpha_{0.5})$ and $p(u)/p(u_{0.5})$ versus fraction of decomposition (α) for BDPINH

3.4 Thermodynamic parameters

Thermodynamic parameters for the compound were calculated using relevant equations **(6-9)** and the results are presented in Table **5** and shown in Fig. (6) The negative entropy value, along with a positive Gibbs free energy, indicates that the decomposition process is endothermic, involving the absorption of heat during the breakdown of the compound and summary of decomposition of BDPINH in the nitrogen under non-isothermal condition are displayed in the Table 6**.**

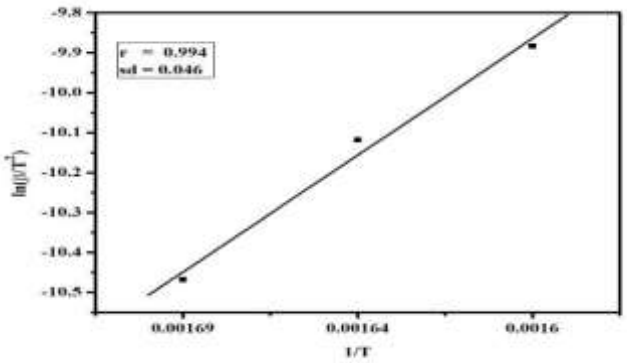

Fig .(6). Plot of $\ln(\beta/T^2)$ versus 1/T for BDPINH

Table 5, Thermodynamic parameters of BDPINH under non-isothermal condition (DTG peak temperature)

β °C/min	Temperature K	lnA (A/min)	E_a kJ/mol	ΔS J/kmol	ΔH kJ/mol	ΔG kJ/mol
10	530.02			-56.75	85.45	115.65

15	556.31	24.21	89.88	-57.13	85.24	117.08
20	567.17			-57.30	85.15	117.81

Table 6, Summary of thermal decomposition of BDPINH in the nitrogen under non-isothermal condition.

	Friedman	KAS	FWO
Isoconventional method E_a kJ/mol	91.88 ± 2.11	94.31± 0.21	96.06 ± 0.21
Kinetic model g(α)	[(1−α)ln(1−α)]+α (D2)		
Invariant kinetic parameters	E_a kJ/mol	89.07 ± 8.3	
	lnA/min	16.55 ± 1.8	

CONCLUSIONS

The studied compound decomposes in a single stage accompanied by heat absorption. The decomposition mechanism follows the D2 model. The compound exhibits low thermal stability, and the activation energy determined by model-free methods closely matches the E_a obtained from thermodynamic parameters. The negative entropy value indicates that the compound decomposes into a more ordered state in the transition state. The positive Gibbs free energy suggests that the decomposition is an endothermic and non-spontaneous process, which is consistent with the observations from TG-DTG/DTA analyses.

LIST OF ABBREVIATIONS

TG	=	Thermogravimetric Analysis
DTA	=	Differential Thermal Analysis
DTG	=	Differential Thermalgravimetric Analysis
KAS	=	Kissinger-Akahira-Sunnose
FWO	=	Flynn-Wall-Ozawa
TLC	=	Thin Layer Chromatography
MHz	=	Mega Hertz
TMS	=	Tetramethylsilane
NH_4OAc	=	Ammonium acetate
ppm	=	Parts per million
μg	=	Microgram
BDPINH	=	N-(3-butyl-2,6-diphenylpiperidin-4-ylidene)isonicotinohydrazide
AKM	=	All Kinetic Model

CONSENT FOR PUBLICATION

Not applicable.

AVAILABLE OF DATA AND MATERIALS

Not applicable

FUNDING

None.

CONFLICT OF INTEREST

The authors declare that no conflict of interest, financial or otherwise.

ACKNOWLEDGEMENTS

The Authors pay sincere gratitude to Department of Chemistry, Annamalai university for IR spectrum and thermal analyzer, STA 7200, Hitachi HTG, Andhra Pradesh for TG, DTA and DTG analyses.

SUPPLEMENTARY MATERIALS

Supplementary materials has included along with the article.

REFERENCES

[1] Thiyagarajan, S.; Gunanathan, C. Direct catalytic symmetrical, unsymmetrical N,N-dialkylation and cyclization of acylhydrazides using alcohols. *Org. Lett.,* **2020**, *22*(16), 6617-6622. https://doi.org/10.1021/acs.orglett.0c02369.

[2] Kumar, D.; Kumar, N. M.; Ghosh, S.; Shah, K. Novel bis(indolyl)hydrazide-hydrazones as potent cytotoxic agents. *Bioorg. Med. Chem. Lett.,* **2012**, *22* (1), 212-215. https://doi.org/10.1016/j.bmcl.2011.11.031.

[3] Teneva, Y.; Simeonova, R.; Valcheva, V.; Angelova, V. T. *Pharmaceuticals,* **2023**, *16*(4), 484. https://doi.org/10.3390/ph16040484.

[4] González-Baró, A. C.; Pis-Diez, R.; Parajón-Costa, B. S.; Rey, N. A. *J. Mol. Struct.,* **2012**, *1007*, 95-101. https://doi.org/10.1016/j.molstruc.2011.11.037.

[5] Ferraresi-Curotto, V.; Echeverría, G. A.; Piro, O. E.; Pis-Diez, R.; González-Baró, A. C. *Spectrochim. Acta, Part A.,* **2015**, *137*, 692–700. https://doi.org/10.1016/j.saa.2014.08.095.

[6] Anagnostopoulos, A.; Matthews, R. W.; Walton, R. A. Studies on metal carboxylates. Part II. Cobalt(II) and Nickel(II) complexes of certain pyridine carboxylic acids and pyridine-3-sulfonic acid: Magnetic and spectral studies. *Can. J. Chem.,* **1972**, *50* (9), 1307-1314. https://doi.org/10.1139/v72-205.

[7] Raviglione, M. C.; Dy, C.; Schmidt, S.; Kochi, A. Assessment of worldwide tuberculosis control. *Lancet,* **1997**, *350* (9077), 624-629. https://doi.org/10.1016/S0140-6736(97)04146-9.

[8] Ojha, S.; Bapna, A.; Talesara, G. L. Synthetic and pharmacological studies on some 1-isonicotinoyl-3-methyl-4-(4-substitutedphenyl)-3a,4-dihydro-pyrazolo[3,4-c]pyrazoles and their ethoxyphthalimide derivatives. *Arkivoc,* **2008**, *11*, 112-122. https://doi.org/10.3998/ark.5550190.0009.b11.

[9] Fox, H. H. The chemical approach to the control of tuberculosis. *Science,* **1952**, *116*(3006), 129–134. https://doi.org/10.1126/science.116.3006.129.

[10] Cymerman-Craig, J.; Willis, D.; Rubbo, S.D.; Edgar, J**.** Mode of action of isonicotinic hydrazide. *Nature,* **1955**, *176*, 34-35. https://doi.org/10.1038/176034a0.

[11] Zubrys, A.; Siebenmann, C. O. Antituberculous isonicotinylhydrazones of low toxicity. *Can. J. Chem.,* **1955**, *33* (1), 11-14. https://doi.org/10.1139/v55-003.

[12] Maccari, R.; Ottanà, R.; Vigorita, M. G. In vitro advanced antimycobacterial screening of isoniazid-related hydrazones, hydrazides, and cyanoboranes: Part 14. *Bioorg. Med. Chem. Lett.,* **2005**, *15*(10), 2509–2513. https://doi.org/10.1016/j.bmcl.2005.03.065.

[13] Kakimoto, S.; Yashamoto, K. Studies on antitubercular Compounds. X. Condensation products of aldehydes and acid hydrazides of pyridine group. *Pharm. Bull.,* **1956**, *4*(1), 4–6. https://doi.org/10.1248/cpb1953.4.4

[14] Nolan, C. M.; Goldberg, S. V. Treatment of isoniazid-resistant tuberculosis with isoniazid, rifampin, ethambutol and pyrazinamide for 6 months. *Int. J. Tuberc. Lung Dis.,* **2002**, *6* (11), 952-958.

[15] Keshavjee, S.; Gelmanova, I. Y.; Farmer, P. E.; Mishustin, S. P.; Strelis, A. K.; Andreev, Y. G.; Pasechnikov, A. D.; Atwood, S.; Mukherjee, J. S.; Rich, M. L.; Furin, J. J.; Nardell, E. A.; Kim, J. Y.; Shin, S. S. Treatment of extensively drug-resistant tuberculosis in Tomsk, Russia: A retrospective cohort study. *Lancet,* **2008**, *372* (9647), 1403-1409. https://doi.org/10.1016/S0140-6736(08)61204-0.

[16] Tse, W. C.; Boger, D. L. Sequence-selective DNA recognition: Natural products and Nature's lessons. *Chem. Biol.,* **2004**, *11*(12), 1607-1617. https://doi.org/10.1016/j.chembiol.2003.08.012.

[17] El-Gammal, O. A.; El-Bindary, A. A.; Mohamed, F. S.; Rezk, G. N.; El-Bindary, M. A. Synthesis, characterization, design, molecular docking, anti-covid-19 Activity, DFT calculations of novel schiff base with some transition metal complexes. *J. Mol. Liq.,* **2022**, 346, 117850.https:// doi.org/10.1016/j.molliq.2021.117850.

[18] Hojjati-Najafabadi, A.; Farahbakhsh, E.; Gholamalian, G.; Feng, P.; Davar, F.; Aminabhavi, T. M.; Vasseghian, Y.; Kamyab, H.; Rahimi, H. Controllable synthesis of nanostructured flower-like Cadmium sulfides for photocatalytic degradation of methyl orange under different light sources. *J. Water Process Eng.,* **2024**, *59*, 105002. https://doi.org/10.1016/j.jwpe.2024.105002.

[19] Seabrook, L. J.; Franco, C. N.; Loy, C. A.; Osman, J.; Fredlender, C.; Zimak, J.; Campos, M.; Nguyen, S. T.; Watson, R. L.; Levine, S. R.; Khalil, M. F.; Sumigray, K.; Trader, D. J.; Albrecht, L. V. Methylarginine targeting chimeras for lysosomal degradation of intracellular proteins. *Nat. Chem. Biol.,* **2024**, *20*(12), 1566-1576. https://doi.org/10.1038/s41589-024-01741-y.

[20] Rajeev, D.; MacIver, N. J. Metformin as a Therapeutic agent for obesity-associated immune dysfunction. *J. Nutr.,* **2024**, *154* (9), 2534-2542. https://doi.org/10.1016/j.tjnut.2024.07.001.

[21] McPherson, M. J.; Hobson, A. D.; Hernandez, J. A.; Marvin, C. C.; Waegell, W.; Goess, C.; Oh, J. Z.; Shi, D.; Hayes, M. E.; Wang, L.; Schmidt, D.; Wang, Z.; Pitney, V.; McCarthy, K.; Jia, Y.; Wang, C.; Kang, B. N.; Bryant, S.; Mathieu, S.; Ruzek, M.; Parmentier, J.; D'Cunha, R. R.; Pang, Y.; Phillips, L.; Brown, N. J.; Xu, J.; Graff, C.; Tian, Y.; Longenecker, K. L.; Qiu, W.; Zhu, H.; Liu, W.; Zheng, P.; Bi, Y.; Stoffel, R. An Anti-TNF-Glucocorticoid receptor modulator antibody-drug conjugate is efficacious against immune-mediated inflammatory diseases. *Sci. Transl. Med.,* **2024**, *16*(650), eadd8936. https://doi.org/10.1126/scitranslmed.add8936.

[22] Yuan, Y.; Li, P.; Li, J.; Zhao, Q.; Chang, Y.; He, X. Protein lipidation in health and disease: Molecular basis, physiological function and pathological implication. *Signal Transduct. Target. Ther.,* **2024**, *9*(1), 1-43. https://doi.org/10.1038/s41392-024-01759-7.

[23] Thng, D. K. H.; Hooi, L.; Siew, B. E.; Lee, K. Y.; Tan, I. J. W.; Lieske, B.; Lin, N. S.; Kow, A. W. C.; Wang, S.; Rashid, M. B. M. A.; Ang, C.; Koh, J. J. M.; Toh, T. B.; Tan, K. K.; Chow, E. K. H. A Functional personalised oncology approach against metastatic colorectal cancer in matched patient-derived organoids. *NPJ Precis. Oncol.,* **2024**, *8*(1), 1-17. https://doi.org/10.1038/s41698-024-00543-8.

[24] Qin, Y.; Huo, M.; Liu, X.; Li, S. C. Biomarkers and computational models for predicting efficacy to tumor ICI immunotherapy. *Front. Immunol.,* **2024**, *15*, 1368749. https://doi.org/10.3389/fimmu.2024.1368749.

[25] Markham, L. E.; Koelblen, T.; Chobanian, H. R.; Follis, A. V.; Burris, T. P.; Micalizio, G. C. From Functional fatty acids to potent and selective natural-product-inspired mimetics via conformational profiling. *ACS Cent. Sci.,* **2024**, *10*, 477-486. https://doi.org/10.1021/acscentsci.3c01155.

[26] Véniant, M. M.; Lu, S. C.; Atangan, L.; Komorowski, R.; Stanislaus, S.; Cheng, Y.; Wu, B.; Falsey, J. R.; Hager, T.; Thomas, V. A.; Ambhaikar, M.; Sharpsten, L.; Zhu, Y.; Kurra, V.; Jeswani, R.; Oberoi, R. K.; Parnes, J. R.; Honarpour, N.; Neutel, J.; Strande, J. L. A GIPR antagonist conjugated to GLP-1 analogues promotes weight loss with improved metabolic parameters in preclinical and Phase 1 settings. *Nat. Metab.,* **2024**, *6*, 290-303. https://doi.org/10.1038/s42255-023-00966-w.

[27] Romero, A. H.; Medina, R.; Alcala, A.; García-Marchan, Y.; Núnez-Duran, J.; Leañez, J.; Mijoba, A.; Ciangherotti, C.; Serrano-Martín, X.; López, S. E. Design, synthesis, structure-activity relationship and mechanism of action studies of a series of 4-chloro-1-phthalazinyl hydrazones as a potent agent against *Leishmania braziliensis*. *Eur. J. Med. Chem.,* **2017**, *127*, 606-620. https://doi.org/10.1016 /j.ejmech.2017.01.022.

[28] Derardja, A. A.; Golea, L.; Benali-Cherif, R.; Luneau, D.; Boutobba, Z.; Boumedjane, Y.; Harkat, H. Synthesis, crystal structure, DFT calculations, Hirshfeld surface analysis and molecular docking studies of a new Manganese complex. *SSRN Preprint*, posted August 23, **2022**. https://doi.org/10.2139/ssrn.4191165.

[29] Nagendra Babu, K.; Vallal Perumal, G.; Rajarajan, G.; Manikandan, G.; Thanikachalam, V. Thermal vaporization of (E)-methyl-2-hydroxy-5-(phenyldiazenyl)benzoate under non-isothermal condition in air atmosphere. *Gravida Review J.,* **2023**, 9(11), 550-573.

[30] Noller, C. R.; Baliah, V. The Preparation of some piperidine derivatives by the Mannich reaction. *J. Am. Chem. Soc.,* **1948**, 70(11), 3853-3855. https://doi.org/10.1021/ja01191a092.

[31] Ramya Devi, V. J.; Vallal Perumal, G.; Rajarajan, G.; Sivakumar, K.; Thanikachalam, V.; Kaviyarasu, K. Synthesis, spectral characterization, Anti-cancer activity evaluation, and molecular docking of substituted 1,2-bis(3-butyl-2,6-diphenylpiperidin-4-ylidiene)hydrazone derivatives. *J. Mol. Struct.,* **2025**, 1321 (Part 4), 140147. https://doi.org/10.1016/j.molstruc.2024.140147.

[32] Friedman, H. L. Kinetics of thermal degradation of char-forming plastics from thermogravimetry. Application to a phenolic plastic. *J. Polym. Sci., Part C: Polym. Lett.,* **1963**, *6*, 183-195. https://doi.org/ 10.1002/polc.5070060121.

[33] Flynn, J. H.; Wall, L. A. General treatment of the thermogravimetry of Polymers. *J. Res. Natl. Bur. Stand., Sect. A,* **1966**, *70*, 487-523. https://doi.org/10.6028/jres.070A.043.

[34] Akahira, T.; Sunose, T. Joint convention of four electrical institutes. *Res. Rep. Chiba Inst. Technol.,* **1971**, *16*, 22-31.

[35] Coats, A. W.; Redfern, J. P. Kinetic parameters from thermogravimetric data. *Nature,* **1964**, *201*, 68-69. https://doi.org/10.1038/201068a0.

[36] Kissinger, H. E. Reaction kinetics in differential thermal analysis. *Anal. Chem.,* **1957**, *29*, 1702-1706. https://doi.org/10.1021/ac60131a045.

[37] Cordes, H. F. Preexponential factors for solid-state thermal decomposition. *J. Phys. Chem.,* **1968**, *72*(6), 2185-2189. https://doi.org/10.1021/j100852a052.

[38] Barnes, P. A. Comprehensive chemical kinetics, Vol. 22. Reactions in the solid state: Edited by C. H. Bamford and C. F. H. Tipper, Elsevier, Amsterdam, 1980, 340 pp. *Thermochim. Acta,* **1980**, 42(2), 249-250. https://doi.org/10.1016/0040-6031(80)87107-3.

[39] Sokolskii, D. V.; Druz, V. A. Introduction in Theory Heterogeneous Catalysis. *Vyshaya Shkola: Moscow,* **1981**.

[40] Sestak, J. Thermodynamical Properties of Solids. *Academia: Prague*, **1984**.

[41] Criado, J. M.; Pérez-Maqueda, L. A.; Sánchez-Jiménez, P. E. Dependence of the preexponential factor on temperature. *J. Therm. Anal. Calorim.,* **2005**, *82*, 671-675. https://doi.org/10.1007/s10973-005-0948-3.

[42] Vlaev, L.; Nedelchev, N.; Gyurova, K.; Zagorcheva, M. A comparative study of non-isothermal kinetics of decomposition of calcium oxalate monohydrate. *J. Anal. Appl. Pyrolysis,* **2008**, *81*, 253-262. https://doi.org/10.1016/j.jaap.2007.12.003.

[43] Lesnikovich, A. I.; Levchik, S. V. A method of finding invariant values of kinetic parameters. *J. Therm. Anal.,* **1983**, *27*, 89-93. https://doi.org/10.1007/BF01907324.

[44] Lesnikovich, A. I.; Levchik, S. V. Isoparametric kinetic relations for chemical transformations in condensed substances (Analytical Survey). *J. Therm. Anal.,* **1985**, *30*, 237-262. https://doi.org/10.1007/bf02128134.

[45] Vyazovkin, S.; Lesnikovich, A. I. Estimation of the pre-exponential factor in the isoconversional calculation of effective kinetic parameters. *Thermochim. Acta,* **1988**, *128*, 297-300. https://doi.org/10.1016/0040-6031(88)85372-3.

[46] Cai, J.; Li, L. S. Kinetic Analysis of wheat straw pyrolysis using isoconversional methods. *J. Therm. Anal. Calorim.,* **2009**, *98*, 325-330. https://doi.org/10.1007/s10973-009-0325-8.

[47] Mālek, J. The Kinetic analysis of non-isothermal data. *Thermochim. Acta,* **1992**, *200*, 257-269. https://doi.org/10.1016/0040-6031(92)85118-F.

[48] Sbirrazzuoli, N.; Vecchio, S.; Catalani, A. Isoconversional kinetic study of alachlor and metolachlor vaporization by thermal analysis. *Int. J. Chem. Kinet.,* **2005**, *37*, 74-80. https://doi.org/10.1002/kin.20054.

[49] Janković, B.; Manić, N.; Perović, I.; Vujković, M.; Zdolšek, N. Thermal Decomposition Kinetics of Deep Eutectic Solvent (DES) Based on choline chloride and magnesium chloride hexahydrate: New Details on the reaction mechanism and enthalpy–entropy compensation (EEC). *J. Mol. Liq.,* **2023**, *374*, 121274. https://doi.org/10.1016/j.molliq.2023.121274.